remote sensing

MDPI

Article

Development of Chaos Terrain as Subaqueous Slide Blocks in Galilaei Crater, Mars

Nabila Nizam †, Claire Divola †, Mackenzie Day *, An Yin and Seulgi Moon

Department of Earth, Planetary, and Space Sciences, University of California Los Angeles, Los Angeles, CA 90095, USA; nizam@hawaii.edu (N.N.); cdivola@g.ucla.edu (C.D.); yin@epss.ucla.edu (A.Y.); sgmoon@g.ucla.edu (S.M.)

* Correspondence: daym@epss.ucla.edu

† These authors contributed equally to this work.

Abstract: Chaos terrain, expressed as enigmatic blocky landscapes on Mars, has poorly understood origins. Several hypotheses have been put forward to explain chaos terrain formation, but none fully account for the morphologies observed in Galilaei crater, the focus of this study. Previously inferred to be a paleolake, Galilaei crater hosts chaos terrain composed of kilometer-scale, disorganized blocks around the southern and southeastern margin of the crater. Blocks are concentrated near the base of the crater wall, with blocks of decreasing size extending into the crater interior. The crater wall slope in regions where these chaos blocks are present is notably lower than in regions where blocks are absent. Based on the observed morphologies, we propose the chaos terrain in Galilaei crater formed by gravity-driven slope failure and down-slope transport as subaqueous landslides and mass flows, initiated at a time when the paleolake level was still high. We propose and discuss Earth analogs for the observed terrain and use mapping-constrained spatiotemporal relationships to reconstruct the sequence of landform development. Subaqueous landslides represent an uncommonly invoked mechanism to explain chaos terrain on Mars, reinforcing the idea that one mechanism cannot explain the diversity of this enigmatic terrain.

Keywords: Mars; Galilaei crater; chaos terrain; subaqueous slide; analog

Citation: Nizam, N.; Divola, C.; Day, M.; Yin, A.; Moon, S. Development of Chaos Terrain as Subaqueous Slide Blocks in Galilaei Crater, Mars. *Remote Sens.* **2022**, *14*, 1998. https://doi.org/10.3390/rs14091998

Academic Editor: Louis Scuderi

Received: 21 March 2022
Accepted: 14 April 2022
Published: 21 April 2022

1. Introduction

The geomorphological evolution of Mars has resulted in a diverse range of landforms, many of which have clear analogs on Earth. Features such as impact craters, valleys, dunes, and delta deposits form by well-understood processes, and Earth analogs have often been used to better understand their Martian equivalents (e.g., [1–3]). However, not all Martian surface terrains have clear analogs on Earth. For example, "chaos terrain" (sometimes "chaotic terrain") refers to regions of a planetary landscape characterized by irregularly shaped, flat-topped, angular-sided blocks separated by steep valleys [4,5]. On Mars, the blocks forming chaos terrain are typically found in depressions up to several hundred kilometers wide and may include a combination of kilometer-scale mesas and angular knobs forming a disorganized surface pattern (e.g., [6–9]). Chaotic terrains are observed extensively on Mars (e.g., in crater basins, linear troughs, channels) but have few analogs that can be studied on Earth. As a result, several hypotheses exist to explain their formation. Martian chaos terrains have been interpreted to form in association with flooding and outflow channels [10,11], or as part of crustal collapse [11,12]. Multiple hypotheses have been proposed to further explain the initiation of crustal collapse to form chaos terrain, including (1) rapid release of groundwater from the rupture of pressurized aquifers [12,13], collapse of subsurface caverns [14], or after a large impact [15], (2) destabilization and collapse of a caldera [16], (3) melting of subsurface ice [17], potentially from magma-ice interactions [7,13,18], and (4) the dewatering of hydrous minerals due to heat from igneous

activity [19]. Each of these chaos terrain formation mechanisms relies on the removal of subsurface material to create accommodation space in which the block pattern can form.

The myriad of proposed formation mechanisms reflects the diversity of chaos terrain morphologies and geologic settings on Mars and suggests that multiple chaos terrain formation mechanisms likely contributed to the modern landscape. Each previously proposed mechanism is supported by examples of chaos terrain on Mars, but no single formation mechanism can explain every instance of chaos terrain observed on Mars Understanding chaos terrain is hindered by the scarcity of analogous terrains on Earth. In this work, we propose a mechanism for chaos terrain formation where subsurface material removal is not needed, based on comparison between morphologies seen in terrestrial subaqueous slides and in Galilaei crater on Mars. The chaos terrain found in Galilaei crater's interior is morphologically inconsistent with previously hypothesized requirement of most chaotic terrain formation mechanisms, as it occurs at a small scale and is not clearly associated with a crustal collapse feature or subsurface material removal. In this study, we address the enigmatic chaos terrain and its geologic context and propose an explanation and terrestrial analog for the development of this Martian chaos terrain.

2. Study Area

Galilaei crater is approximately 137 km in diameter and is located in the Margaritifer Terra region of Mars at 5.7°N, 333.0°E (Figure 1). The size of Galilaei crater suggests it should possess a central uplift peak [20] and widespread ejecta blanket [21]. The absence of both of these features reflects the significant modification of the surface post-impact. The cratered plains that surround Galilaei crater have been previously interpreted as a part of the middle Noachian highland unit [22]. In the southwest, this unit borders a Hesperian transition unit and a Hesperian transition outflow unit which extends from the east of Valles Marineris into Chryse Planitia [22]. Galilaei crater lies ~50 km from the Hesperian transition unit, but its interior is topographically connected via Tana Vallis, a channel cut into the southwestern Galilaei crater wall (Figure 1B). Previous work has identified Galilaei crater as a paleolake basin. Coleman (2015) interpreted that Galilaei crater was filled by water entering the basin via channels crossing the rim in the southwest and via breached aquifers responding to the change in overburden [23]. Coleman (2015) further used stratigraphic superposition to infer that Tana Vallis is an outflow channel that developed after filling and caused the paleolake to rapidly drain. Major additional channels to the southwest and northeast of Galilaei crater (e.g., Ares Vallis) originate at chaos terrain (e.g., Aram and Hydaspis Chaos) and drain north towards Chryse Planitia (Figure 1A). In this work, we focus on the blocky, chaotic terrain present in the interior of Galilaei crater. Galilaei crater itself is neither entirely filled with chaotic terrain nor labeled as a martian "chaos", but it sits in a region hosting many prominent chaos terrains including Hydraotes, Hydrapsis, Aurorae, and Aram Chaos, which are all geographically associated with the same system of north-flowing outflow channels.

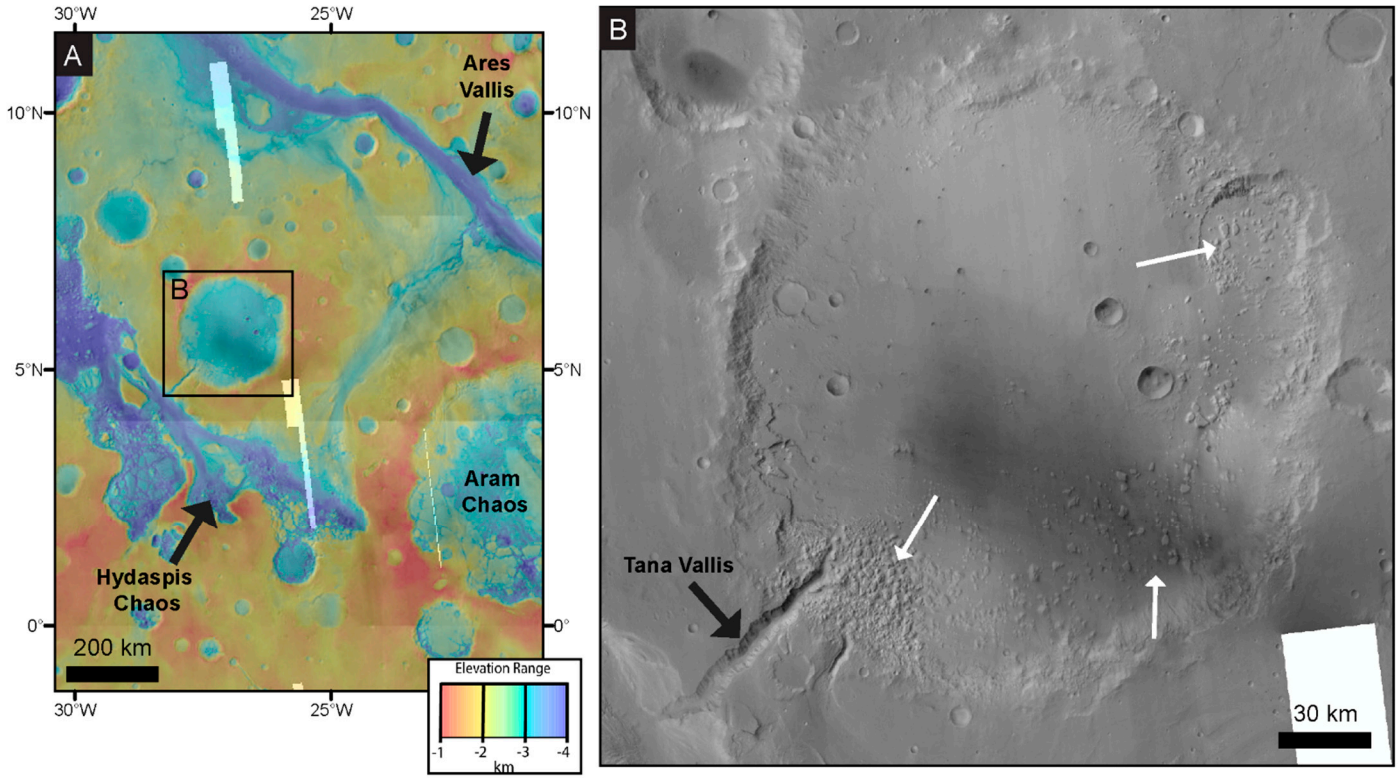

Figure 1. Galilaei crater and its surroundings. (**A**) A colorized elevation map of Galilaei crater (boxed) and the surrounding area. Elevation data are blended MOLA and HRSC at 60% transparency with underlying CTX image mosaic basemap (see Data and Methods). (**B**) Galilaei crater shown in visual image (CTX) mosaic. The crater was a paleolake that drained through the Tana Vallis outflow channel (black arrow) and hosts interior blocks discussed as chaos terrain in this work (white arrows). North is up in all figures.

3. Data and Methods

Galilaei crater and its surroundings were studied using a global mosaic of Mars Reconnaissance Orbiter (MRO) Context Camera (CTX) images [24,25]. The CTX mosaic base map provided sufficient resolution to distinguish between major landforms in the study area. When available, MRO High Resolution Imaging Science Experiment (HiRISE; [26]) images were used to observe the surface in more detail. To understand topography in the study area, we used elevation data with 128 px/deg (463 m/px) resolution from the Mars Global Surveyor (MGS) Mars Orbiter Laser Altimeter (MOLA; [27]) and elevation data collected by the Mars Express High Resolution Stereo Camera (HRSC; [28]) at 75 m/px resolution (Figure 2A). Slope maps were generated from HRSC DEMs using the Slope tool in the Spatial Analyst Toolbox of ArcGIS 10.6.1 (Figure 2B). To better understand the relationship of the chaos terrain in Galilaei crater to other geologic units in the region, we constructed a geomorphic map of the study area (Figure 3). Units were defined based on differentiable surface textures, topography, and morphology. All mapping was conducted using ArcGIS 10.6.1 on CTX base map with disambiguation using MOLA, HRSC, and HiRISE data when necessary and available. To identify mineral species present in the study area, we analyzed spectra from the Compact Reconnaissance Imaging Spectrometer for Mars (CRISM) on MRO using the image processing software Environment for Visualizing Images (ENVI) and the CRISM Analysis Tool [29]. All data used in this work is publicly available and archived on the NASA Planetary Data System.

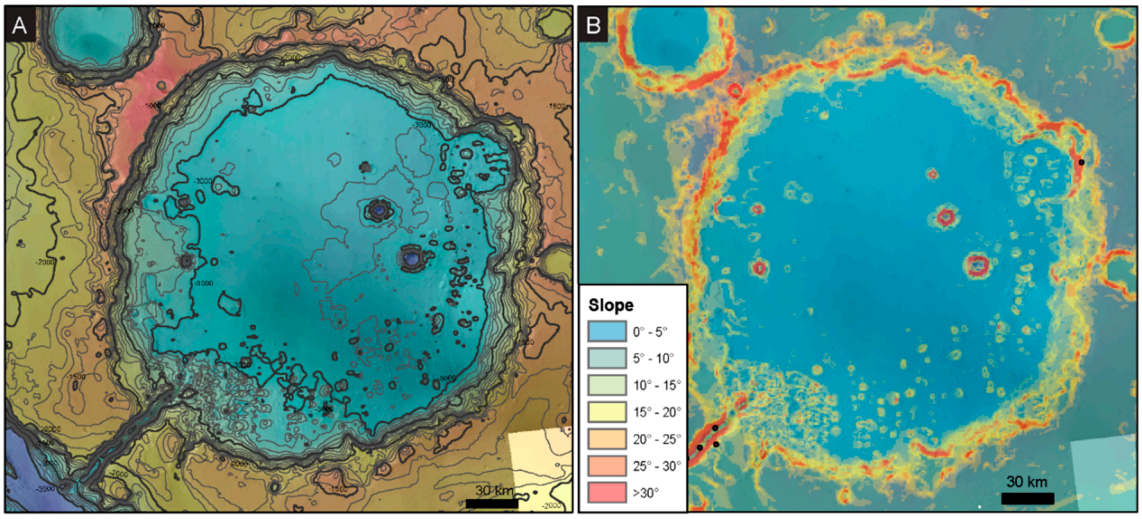

Figure 2. Topography and slopes in Galilaei crater. (**A**) A colorized elevation map of Galilaei crater (see color bas in Figure 1A) with overlain elevation contours. Contour interval is 100 m, and elevation data is derived from HRSC. Note the <100 m relief on most of the crater floor. (**B**) Slope map of the study area generated from the DEM in (**A**). Slopes are highest along the crater wall and outflow channel (Tana Vallis) walls. The crater wall in the northwest of the crater, where chaos blocks are absent from the crater floor, is notably steeper than the southeastern crater wall, where chaos blocks are abundant.

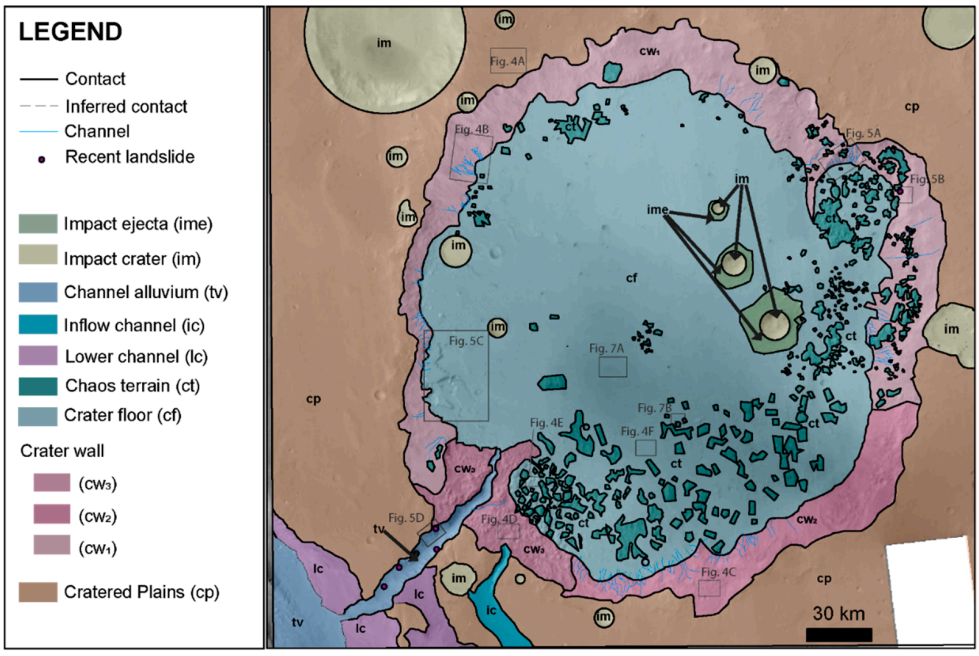

Figure 3. Geomorphic map of Galilaei crater and its surroundings. Units and unit boundaries are shown partially transparent over CTX mosaic basemap. Note that the chaos terrain is preferentially near the crater wall and dominantly in the south and southeast of the crater interior, east of the Tana Vallis outflow channel (tv). Locations of subsequent figure panels are boxed and labeled.

To estimate the surface age of major geomorphic units in Galilaei crater, we measured craters >100 m in diameter within the study area. Small craters are obliterated on Mars over geologic time and can be difficult to resolve in CTX images. The 100 m diameter threshold was chosen to avoid ambiguity in resolvability and minimize the influence of obliteration, while still having a statistically significant number of craters to use in age

estimate analysis. Crater density measurements were used to estimate the surface age of the crater floor and surrounding plains using the Craterstats tool [30,31] with a Martian epoch boundary times of Michael (2013) [32], chronology system and function (CF) from Neukum and Ivanov (2001) [33] and Hartmann and Neukum (2001) [34], production function (PF) from Ivanov (2001) [35], and equilibrium function (EF) from Hartmann (1984) [36]. Crater density was measured on the two largest mapped units to provide a statistically significant number of small and large diameter craters. To assess the influence of resurfacing, we further divided the crater distributions into small (<2 km diameter) and large (>2 km in diameter) craters and reported the age based on each group separately. Causes of disagreement between the age estimated from large and small craters are discussed in general by previous authors [32,37,38] and explored for our study area below.

4. Observations and Results

4.1. Contextual Geomorphic Mapping and Crater Interior Geomorphology

Evidence for the origin of the chaos terrain comes from observations of the blocks themselves and context from the local related landforms. The photogeomorphic map of Galilaei crater highlights five major components of the local landscape (Figure 3): the cratered plains surrounding Galilaei crater (cp), the crater wall (cw_1, cw_2, cw_3), the crater floor (cf), the chaos terrain (ct), and channels (tv, lc, ic). Superimposed across the study area are small impacts (im) and their ejecta (ime) that sometimes obscure the underlying geology and so have been mapped separately in Figure 3. The geographic distribution and surface textures of each mapped unit provide local geomorphic context to the chaos terrain and some clues to its formation mechanism.

The oldest terrain in the study area is the cratered plains unit (cp), characterized by a homogenous surface tone, low-relief (<100 m scale) undulations in topography with kilometer-scale wavelengths, and a high density of craters with rounded rims (Figure 4A). The cratered plains unit surrounds Galilaei crater and is truncated by incised channels in the southwest of the study area. Craters smaller than 1 km in diameter on this unit are present and resolvable but exhibit no visible ejecta. Few craters larger than 1 km are present, some of which display ejecta blankets.

Galilaei crater truncates the cratered plains unit. No clear ejecta are resolvable today from the initial impact. The crater is approximately circular in plan-view, but as compared to pristine craters, the crater margins are irregular and exhibit varying slopes along the crater wall (as calculated from HRSC DEM) predominantly below the angle of repose (30°; Figure 2B). The rim of Galilaei crater is only slightly raised with respect to the surrounding plains. Local relief on the rim is highest at the northwest margin of the crater (~500 m above the surrounding plains), but most of the crater rim exhibits little to no relief with respect to the surrounding plains (<100 m in the northeast). The total relief on the wall with respect to the crater interior (i.e., the modern depth of the crater) is ~1.5 km. The surface texture of the interior crater wall (cw) exhibits variable slopes with irregular undulations and rounded topography. Variations in crater wall expression can be grouped into three categories: smooth crater wall (cw_1, Figure 4B), chaotic crater wall (cw_2, Figure 4C), and highly chaotic crater wall (cw_3, Figure 4D). The smooth crater wall unit (cw_1) has surface slopes predominantly $\geq$30° with few to no overlying block or knobs and constitutes the largest portion of the crater wall. Small channels (the largest measuring 0.6 km wide, and 5.1 km long) have been cut into this sub-unit of the crater wall at various positions (Figure 5A; mapped in blue in Figure 3). A landslide within the smooth crater wall unit has a total length (head to toe) of 3.8 km, and its toe displays a flat-topped block resembling the chaos terrain blocks seen on the crater floor (Figure 5B). However, the landslide toe block displays more well-defined edges and less rounded marginal slope blocks in the chaos terrain. Impact craters can be seen superimposed on the landslide toe.

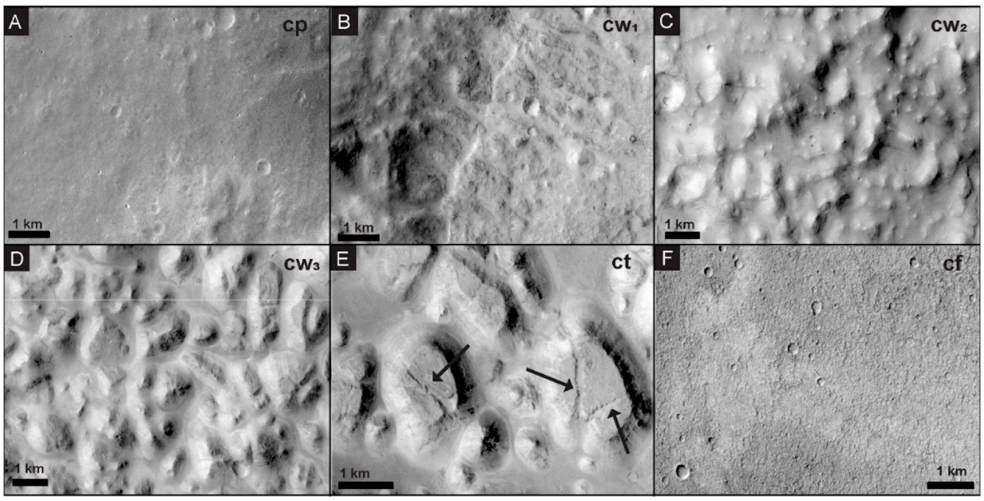

Figure 4. Example images of the geomorphic units mapped in Figure 3. (**A**) Cratered plains (cp) that surround Galilaei crater host eroded craters and low-relief topography. (**B**) The smooth crater wall (cw_1) subunit dominates the northern and western crater rim and is incised by small channels. (**C**) the chaotic crater wall (cw_2) subunit exhibits sub-kilometer-scale rounded knobs similar to highly eroded chaos terrain. (**D**) The highly chaotic crater wall (cw_3) subunit includes flat-topped blocks similar to small chaos blocks observed further into the crater basin. (**E**) Chaos terrain (ct), the focus of this work, is defined by irregularly shaped, often flat-topped, blocks and knobs. In some cases, fractures show where the flat-topped block has broken apart (arrows). (**F**) The crater floor (cf) hosts many small craters with slightly sharper rims than seen on the surrounding plains. Topography on the crater floor is limited. All images are contrast-stretched CTX. See Figure 3 for image locations.

The chaotic crater wall sub-unit (cw_2) is differentiated by the presence of superimposed rounded mounds and knobs on the wall, morphologically similar to eroded chaos terrain (Figure 4C). The knobs are rarely present near the top of the crater wall and are instead concentrated 1.5 km to 4 km downslope in this subunit. The chaotic crater wall unit (cw_2) dominates the southeastern crater wall and mostly exhibits surface slopes of <20°, with a few areas of higher slopes, ≥30° (Figure 2B). The final subunit, the highly chaotic crater wall (cw_3), is differentiated by blocks and knobs that fully cover the wall surface, and frequently exhibit flat tops, not just rounded eroded surfaces (Figure 4D). Highly chaotic crater wall terrain dominates the region around the outflow channel at the head Tana Vallis. Surface slopes on this subunit are primarily <15°, with some isolated regions of higher slope (Figure 2B). Crosscutting the northeastern rim of Galilaei crater is a ~23 km diameter crater that is only differentiable by the circular pattern deviation in the trend of the Galilaei crater rim. Heavily reworked, similar to Galilaei crater, this 23 km diameter crater created a small mini-basin within Galilaei crater that can still be seen and is defined by the smaller crater rim (Figure 6A).

The crater floor (cf) was previously assigned by Tanaka et al. (2014) to be a late Hesperian transition unit. In the crater interior, the unit is defined by smooth surface texture as compared to the surrounding plains, with only meter-scale, long-wavelength variations in topography (Figure 4F). The surface slope throughout the crater floor is consistently <5° (Figure 2B), forming a relatively flat plain within the crater interior. The crater floor is dotted with smaller craters, the largest of which (maximum ~11 km in diameter) are associated with still resolvable ejecta and are mapped in Figure 3. Other than small craters, the most abundant features on the crater floor are chaos terrain blocks (Figure 4E). Understanding the formation of these chaos blocks is the focus of this work. Therefore, the chaos unit (ct) is discussed in detail in Section 4.2. At the lowest elevation within the crater floor, we observed a polygonal pattern on the surface that is interrupted by chaos terrain blocks and similarly shaped depressions (Figure 7; Section 4.2). Northwest of the head of Tana Vallis, the crater floor hosts a sharp-edged depression delineated scarps up to a few hundred

meters deep (Figure 5C). Chaos terrain knobs and blocks are largely absent in this area. Previous work called these regions 'collapsed ground' and attributed their formation to the rupturing of a subsurface aquifer beneath the crater floor or exposed in the crater walls [23]. CRISM images covering the crater walls, floor, and chaos blocks were analyzed using standard methods (e.g., following [39–41]). Hydrated mineral signatures were specifically investigated, but no mineralogical signatures sufficiently distinct from martian dust were resolvable in any of the images (image IDs: FRT 0001EBDD, HRL 00019B5F, and HRL 00006547).

A large outflow channel cuts across the cratered plains unit, dissecting the rim and wall of Galilaei crater and connecting the crater floor unit to the larger outflow features of Hydaspis Chaos to the southwest. The outflow channel, formally named Tana Vallis (tv), is ~56 km-long with a width of ~1.5 km at the crater wall, increasing to ~6 km as it moves away from Galilaei crater. The walls of this outflow channel (tv) maintain steep slopes $\geq 30^{\circ}$ (Figure 2B). Transverse aeolian ridges occur widely on the floor of Tana Vallis, and several lobate flow features, interpreted by previous works as paleo-landslides [23], are present at the base of the channel walls (Figure 5D). The landslides in Tana Vallis differ in morphology from landslides on the smooth crater wall (Figure 5B). The toes of landslides in the Vallis present a more rounded, lobe shape that extends out like a fan, not maintaining the block shape seen in crater wall slides. These toes do not resemble the chaos blocks seen within Galilaei crater and display few to no superimposed craters.

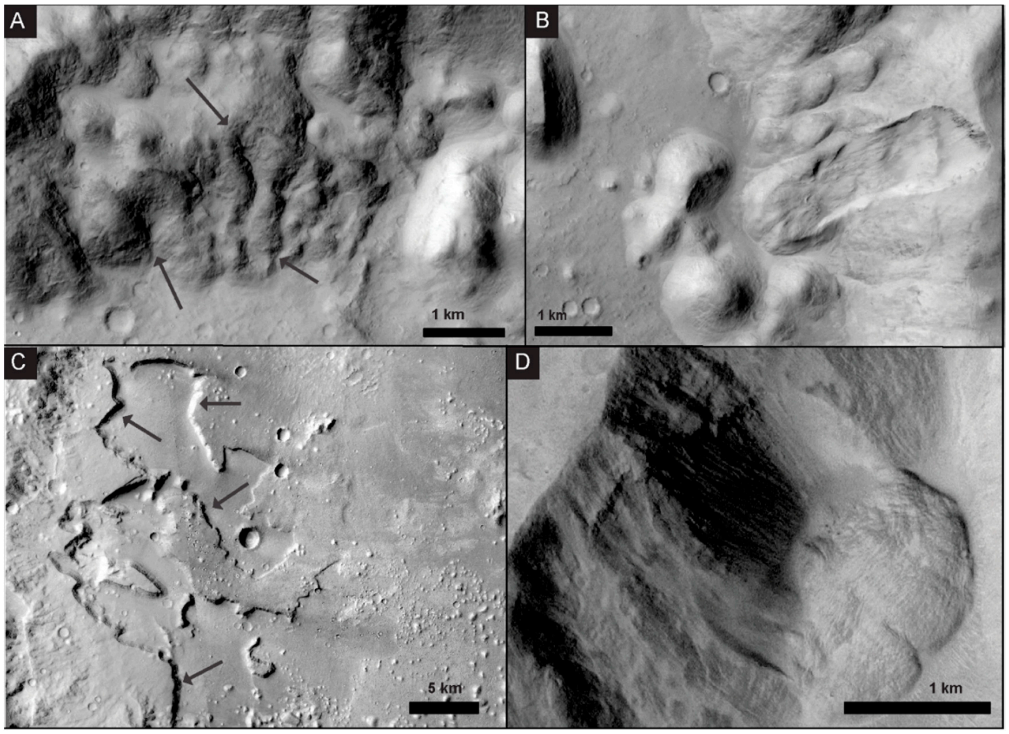

Figure 5. Erosion across Galilaei crater. (**A**) Channels (arrows) are commonly carved into the Galilaei crater rim and could have been pathways for water to fill the paleolake. (**B**) A landslide in the wall of Galilaei crater with the head scarp and toe still intact. The toe of the landslide maintains a flat-topped blocky morphology seen in many chaos terrain blocks within the crater. (**C**) Steep-walled depressions in the western Galilaei crater interior. Steep scarps (arrows) line depressions in a region largely devoid of chaos terrain blocks. (**D**) A landslide in the steep walls of the Tana Vallis outflow channel. See Figure 3 for image locations.

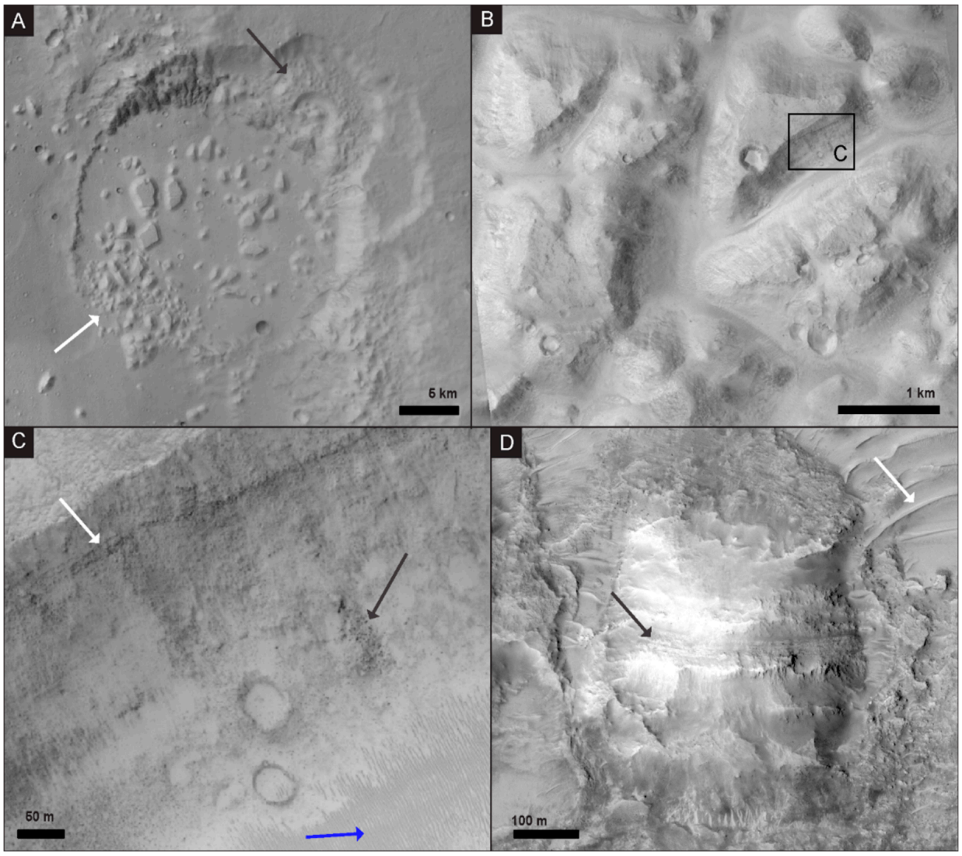

Figure 6. Chaos terrain in Galilaei crater. (**A**) A 23 km diameter crater interrupts the rim of Galilaei crater and is itself filled with chaos terrain blocks. The northwest of the smaller crater rim (black arrow) is particularly eroded and is potentially a source for blocks that were transported to the southwest. The southwestern rim of the crater (white arrow) may have provided a topographic barrier that prevented the blocks from sliding further, as supported by the cluster of blocks inside the crater at this point and the absence of blocks exterior to this crater rim. (**B**) The typical block and mound morphology of chaos terrain in Galilaei crater. The location of (C) is boxed. (**C**) The wall of a chaos block shows superimposed boulders (black arrow) and a resistant layer (white arrow) near the surface of the flat-topped block. Modern aeolian bedforms occupy the base of the valley (blue arrow). (**B**,**C**) are from HiRISE image ESP_033088_1850. (**D**) A mound in the chaos terrain shows sub-vertically exposed layering (black arrow), suggesting the block was tilted during transport. Modern aeolian bedforms (white arrow) again occupy topographic lows. HiRISE image ESP_068377_1855.

In addition, southeast of Tana Vallis is a shallower channel that cuts across the cratered plains and dissects the rim of Galilaei crater. Previous work interpreted this as an inflow channel (ic; [23]) at least partially responsible for the filling of Galilaei crater with water to make it a paleolake. The width of the inflow channel decreases heading north towards Galilaei crater from ~6 km on its southern end to ~2 km as it reaches the crater wall. To the south of the channel mouth, smooth lineations are seen in the widest portion of the channel before the surface texture transitions downstream into a smooth-floored, steep-walled channel that then loses definition further into the crater as it transitions into the highly chaotic crater wall unit (cw_3). The inflow channel trends parallel to the larger-scale outflow channel related to Hydaspis Chaos in the southwestern corner of the study area, which we delineate as the lower channel unit (lc).

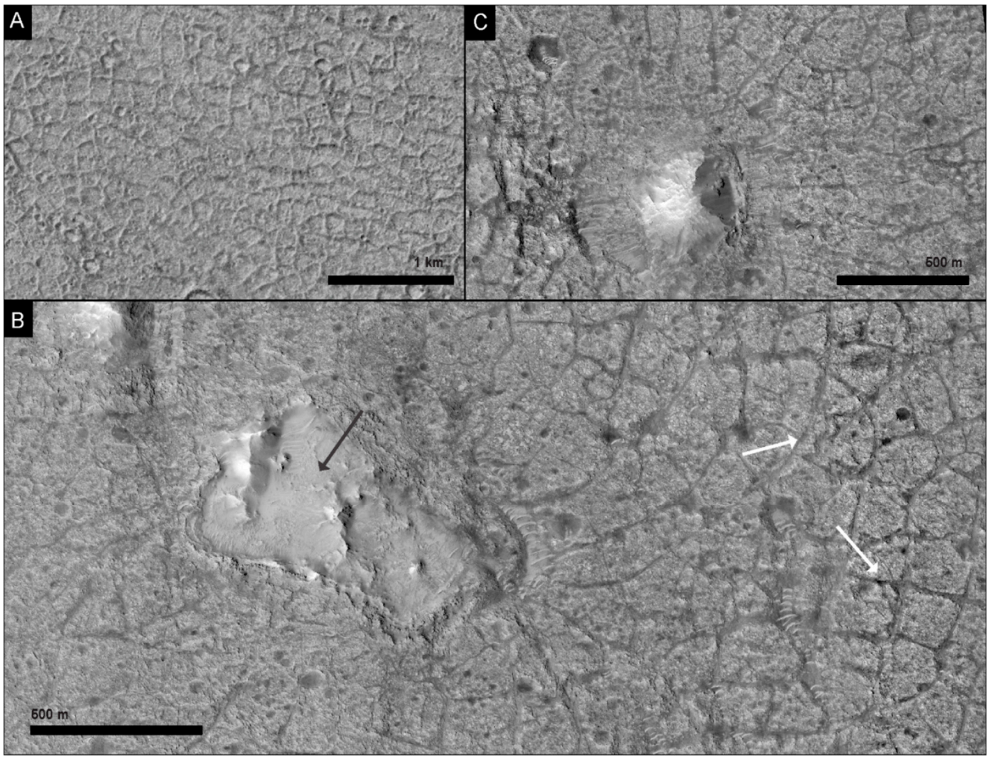

Figure 7. Polygonal patterns in the lowest elevation interior of Galilaei crater. (**A**) Polygonal terrain with raised ridges defining the polygons. CTX Image mosaic basemap. (**B**) Polygonal terrain defined by negative relief fractures in the surface (white arrows) is sometimes interrupted by depressions (black arrow) at the same scale as the chaos blocks. Erosion after the drying of Galilaei crater may have removed block material, leaving the depressions behind. (**C**) Fractures in the polygonal terrain radiate outward from a small mound that is part of distal chaos terrain. (**B**,**C**) are from HiRISE image ESP_068377_1855.

4.2. Chaos Terrain

Chaos terrain is defined and identified by irregularly-shaped, variably-sized, roughly polygonal blocks and mounds that on Mars are most commonly found in depressions [5]. In Galilaei crater, the blocks that form the chaos terrain are abundant, but are not uniformly distributed across the crater interior. The majority of chaotic blocks are found on the southeastern half of the crater, distributed near the rim and extending into the basin (Figure 6). Chaos blocks range from 100 m–3 km in width and stand 100 m–300 m in height. Individual blocks >1 km in width are found only on the crater floor, often with kilometer-scale spacing separating them, while blocks located on the crater wall are commonly clustered closer together and are smaller than 1 km in size. Qualitatively, the blocks decrease in size as they increase in distance from the crater wall (Figures 3 and 6A). Blocks with a width between 1 km and 2 km are seen as far as 29 km from the base of the crater wall, while smaller blocks are prevalent up to 56 km away from the base. The largest chaos blocks are not present on the slope of the crater wall itself, nor are they common near the head of Tana Vallis. Near Tana Vallis, the density of blocks is high, almost fully covering the crater floor, but the block size is smaller (predominantly, a few 100 m scale) than at other locations of similar distance into the crater from the rim. We note that the southern and northern portions of the crater wall differ by the presence and absence of chaos terrain, respectively, but also have notably different slopes. Chaos terrain is associated with parts of the crater wall that have slopes below the angle of response.

The margins of the individual blocks are steep but not vertical, with slopes up to the angle of repose (~30°) commonly covered in loose clasts and other evidence of mass wasting (Figure 6C). Blocks greater than 1 km wide often exhibit flat tops. Many retain

visible impact craters on these upper surfaces, and some blocks show subordinate fractures secondary to the margin of the blocks themselves (Figure 4E). Blocks that do not have flat tops exhibit fewer visible impacts. An erosionally resistant layer protrudes from some of the blocks, typically parallel to the block surface at ~50 m below the surface (Figure 6C). The resistant layers are most commonly observed in the larger (>1 km wide), flat-topped blocks. In one instance, bedding in a block is sub-vertically oriented, suggesting the chaos block had tilted during its formation (Figure 6D). At the base of many of the chaos blocks, boulders are visible, some reaching upwards of 3 m in diameter (Figure 6B). In some areas between the chaos blocks, we observed transverse aeolian ridges (TARs). As is typical of TARs on Mars, the bedforms spanned the local valley topography between chaos blocks and exhibited orientations controlled by this topography [42,43].

The chaos blocks are superimposed on the crater floor unit, which is tonally homogenous and exhibits almost no topographic relief. South of the crater center, near the lowest elevation in the basin (−3080 m to −3120 m), the surface texture of the crater floor changes to exhibit polygonal patterns of either fractures or raised ridges (Figure 7). In the region where polygons are present (~50 km^2), the raised ridge morphology dominates the west and the fracture morphology dominates the east. Polygons with raised rims have an average diameter of 163 m ± 34.8 m (Figure 7A). Polygons with negative relief margins (fractures) average 119 m ± 34.9 m in diameter (Figure 7B). Impact craters are observed in the polygonally textured region of the crater floor but are qualitatively less dense than elsewhere on this unit.

Chaos terrain blocks are present where the negative relief, fracture-margin polygons occur, but were not observed alongside the raised ridge polygonal terrain. Where chaos blocks and polygonal terrain are present together, the fractures defining the polygon edges seem to radiate outward from the chaos blocks (Figure 7C). The chaos blocks themselves sit in ~5 m deep depressions that interrupt the polygonal fractured terrain. Some of these depressions are incompletely filled by the chaos blocks or are entirely empty (Figure 7B). Where open space or moats around the blocks are present in depressions, transverse aeolian ridges are commonly present in the topographic lows.

4.3. Impact Crater Chronology

To estimate the surface age of geomorphic units in Galilaei crater, we mapped all craters greater than 100 m in diameter within the crater floor unit and on the surrounding cratered plains outside Galilaei crater. The extent of most of the mapped geomorphic units was too small to support a statistically robust estimate of surface age, therefore, age was only estimated for the crater floor (cf) and cratered plains (cp) units. The crater floor unit and cratered plains unit cover 9584 km^2 and 10,145 km^2, respectively. Note that the chaos terrain found in Galilaie crater was mapped separately and is not included in the crater floor age estimate. A total of 8430 craters were mapped on these two units, 5231 on the crater floor unit and 3199 on the cratered plains. Using the open-source program Craterstats [30,31], we plotted the cumulative crater density with respect to crater diameter and fit curves to these data. Ages were estimated by comparing the fit curves against isochrons generated with a chronology function (CF) [34], production function (PF) [35], and epoch system [32].

Using the largest craters in the study area (>2 km in diameter), the estimated surface age of the crater floor unit was 3.7 Ga, and that of the cratered plains was 3.9 Ga (Figure 8). Craters <2 km in diameter follow a notably younger isochron slope as compared to the density of larger craters. Using these smaller craters alone, the estimated ages for the crater floor and cratered plains units were 1.4 Ga and 1.3 Ga, respectively. The significantly younger age reflected in the smaller craters is a common phenomenon on Mars and likely reflects resurfacing events that obliterated some small craters, but were insufficient to entirely obliterate craters >2 km in diameter (e.g., as discussed in [44–47]). Given the geologic context of Galiliae crater, such processes could have included aeolian, fluvial, impact, thermal, or cryogenic alteration.

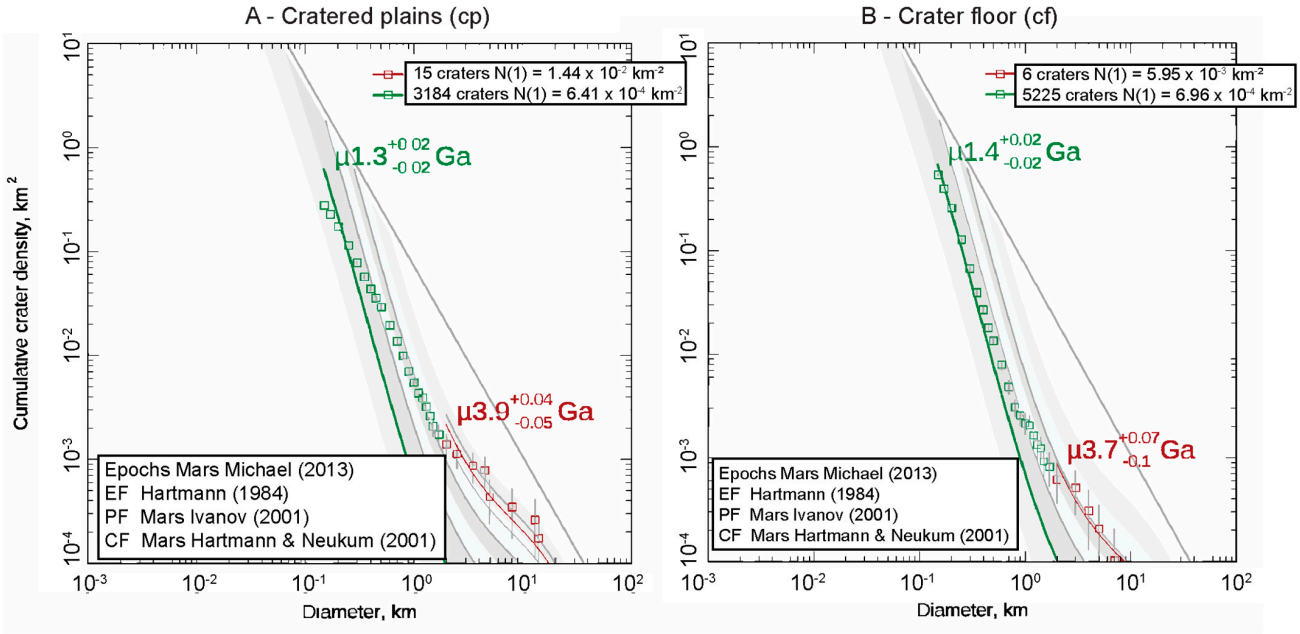

Figure 8. Surface age estimates using crater size frequency distributions. (**A**) Craters measured in the cratered plains (cp) unit are compared against standard isochrons. (**B**) Craters measured in the crater floor (cf) unit reflect a similar age to the cratered plains in (**A**). Both plots were generated using Craterstats open-source software using craters >100 m in diameter.

5. Discussion

5.1. Inconsistency with Previously Proposed Chaos Formation Mechanisms

The morphology and geologic context of chaos terrain in Galilaei crater are inconsistent with many previously proposed mechanisms of chaos terrain formation. The most commonly proposed chaos formation mechanisms rely on crustal collapse via removal of material from the subsurface [7,12–14,16–19]. Although this mechanism well-explains the morphology of depression-filling blocks observed elsewhere on Mars, the floor of Galilaei crater is non-uniformly covered with blocks and knobs, inconsistent with formation by material removal from below. Evidence of crustal collapse in Galilaei crater is potentially present in the northwestern crater floor, where steep-walled scarps surround depressions in the crater floor (Figure 5C). However, these depressions are notably distant from the majority of the chaos terrain.

In previous work on the hydrologic history of Galilaei crater, Coleman (2015) proposed that the incision of inflow channels in the southwest of Galilaei crater locally thinned the cryosphere, causing subsurface aquifers to rupture and form the observed chaos terrain [23]. This would suggest that the locations of the developing chaos blocks should be mediated by the extent of the aquifer and/or the locations of infill channels. The largest channel that likely delivered water into Galilaei crater is located just south of Tana Vallis, but smaller channels dissect the crater rim at all positions around the crater margin. Given that the chaos terrain is not closely spatially associated with either the large or small channels, the above hypothesis would suggest that the extent of the blocks is related to the extent of the subsurface aquifer. This latter idea is difficult to disprove, and although the mechanism proposed by Coleman (2015) is possible and consistent with the observed morphologies, we argue that cryogenic processes are not strictly necessary to form the chaos terrain. Galilaei crater is established as being a paleolake with a near-rim water level before the incision of the Tana Vallis outflow channel [23], consistent with the Martian climate at the time. When the water level was high, the steep crater walls would have become saturated with water. We propose that the steep crater wall topography and high water level provide ideal conditions for the formation of subaqueous landslides and on their own can explain the chaos terrain in Galilaei crater with a gravity-driven mechanism of slope failure. No

subsurface aquifers or cryosphere are necessary, though we note that the proposed model does not disallow their presence. Below we compare the Galilaei crater chaos terrain to subaqueous mass movement on Earth and discuss specific analogs for the terrain.

5.2. Subaqueous Mass Flow Analogs for Chaos Terrain on Earth

The morphology and distribution of the chaos blocks seen in Galilaei crater resemble subaqueous continental shelf landslides on Earth, such as the Palos Verdes slide in California or the Nuuanu and Wailau debris avalanches in Hawaii. These two subaqueous gravity-driven slope failures exhibit many of the same geomorphological characteristics as the chaos blocks in Galilaei crater and are by no means the only such examples (see reviews in [48,49]). In the Palos Verdes slide located on the San Pedro escarpment in California, the lower slope exhibits blocky debris emplaced after a slope failure along the upper section of the escarpment [49,50]. Debris were seen as far as 8 km out from the base of the 600 m-high slope, deposited as flat-topped and rounded sedimentary blocks that had slid along down the slope and along the surface ([51]; Figure 1 of [50]). The Nuuanu and Wailau volcanic flank debris avalanches (Figure 9A) formed off the northwest coast of Oahu and Molokai islands of Hawaii, display a similar morphology as Palos Verdes and Galilaei crater of disconnected, flat-topped sedimentary blocks in this case extending 200 km from the headwall position [52–55]. The blocks maintained rugged margins with steep slopes, scattering across the underlying plain in a range of block sized and shapes. Previous authors noted that the size of the blocks in this example decreases with distance away from the source [48,56], as is also the case, qualitatively, in Galilaei crater (Figure 9B). The block margins are steep but subvertical. The largest block in the Hawaiian example, known as the Tuscaloosa seamount, is approximately 25 km wide and 12 km long, located nearly 100 km from the northern shore of Oahu Island [53,54]. The Tuscaloosa seamount shares similarities with the largest blocks on the Galilaei crater floor in that both are flat-topped with rounded margins and similar steep slopes on all sides [54].

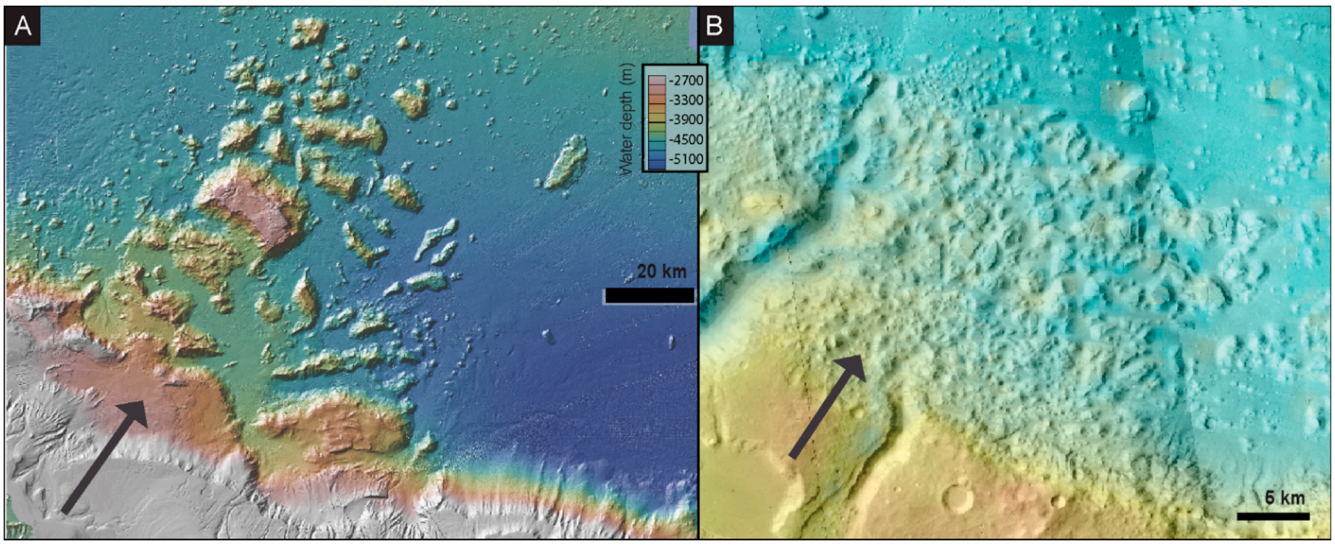

Figure 9. Subaqueous mass flow Earth analog. Black arrows in this figure illustrate the direction of the slide from the region of interpreted slope failure toward the transport direction and deposit. (**A**) Subaqueous landslide analog from Nuuanu and Wailau landslide on the west coast of Oahu, Hawaii. As with Galilaei crater, the deposit is composed of disorganized blocks, the largest of which are flat-topped, and the blocks qualitatively decrease in size in the transport direction. Image from the generic mapping tool [57]. (**B**) Chaotic terrain in Galilaei crater interpreted to have originated from subaqueous landslides (as in (**A**)).

The underlying slopes in the Hawaiian example on which the subaqueous deposits slid were measured as 7.3° for the Nuuanu landslide and 6.1° for the Wailau landslide, with steeper slopes present at the shelf break. Similar or lower slopes are common in subaqueous landslide runouts, with the area of initiation always having a higher slope [48,58,59]. In a study of submarine landslides along continental slopes off the US [60], unfailed slopes adjacent to observed slides were measured and reported to average 16.3° near Oregon, and ~4° near California, New Jersey, and the Gulf of Mexico. On Mars, crater walls in fresh craters can be at or above the angle of repose and rapidly degrade over time (e.g., [61,62]). In Galilaei crater, the modern crater wall slopes range from ~5° to >30°, well above the steepnesses needed to initiate a mass flow. The crater wall closest to the chaotic terrain, along the southern and southeastern rim, exhibit slopes predominantly 15°–20°, as composed to the higher slopes on the northern section of the crater wall, ranging from 28° to 35° (Figure 2). The difference between steep crater wall slopes in areas without chaos terrain and shallower slopes where chaos terrain is present is most easily explained by the downslope movement of material at the crater rim, causing the rim to shallow and causing the removed material to be deposited in the chaos blocks observed. This hypothesis is further supported by observations of chaos terrain inside the 23 km diameter on the northeastern Galilaei crater rim. Here, the small crater rim is heavily eroded, particularly in the northeast. Chaos blocks in the small crater interior are clustered at the southwestern rim of the small crater, potentially where the small crater rim served as a topographic obstacle, preventing the blocks from sliding further.

Various triggers have been identified for subaqueous landslides on Earth, including seismic activity, ground shaking, tsunamis, and tectonic activities from rift zones (see discussion in [49,63,64]). Although not all triggers proposed or identified on Earth can apply to Mars, frequent impacts early in Mars' history would have provided a readily available mechanism of ground disturbance. Previous work has also suggested that impacts may have initiated chaos-terrain-forming ground disturbances [15]. The abundant impact craters on both the Galilae crater floor and surrounding plains suggest many opportunities for this initiation. The non-uniform distribution of slide blocks (present in the south-southeast and absent in the north-northwest) could suggest a non-uniform triggering mechanism or could reflect heterogeneities in the local geology of this area. The relief on the crater rim in both locations is similar (~2 km), and there is no evidence to suggest that the starting crater wall slopes were not the same.

The proposed subaqueous landslide mechanism is most similar to previous interpretations of chaos at the head of channels outflowing into Chryse Planitia [8]. Chaos terrain forming in major outflow channels would have been eroded by flowing water passing around the blocks, unlike blocks formed in Galilaei crater where flow was limited by the topography of the closed basin. The formation of subaqueous slides in the closed basin of Galilaei crater suggests that other morphologies, related to subaqueous landslides on Earth, may be identifiable in this study area where bypassing flow may not have obliterated some surface textures. For example, landslides originating from the crater wall would be expected to leave a path or trail across the surface during formation. Trails from subaqueous landslides are also not typically observed on Earth, but the 25 cm/px resolution of HiRISE images available over the floor of Galilaei crater provides much more detail than the bathymetric data used to image many subaqueous landslides on Earth. However, tracks connecting the putative path of the chaos blocks from the crater wall to their current position were not observed in either HiRISE or CTX images of Galilaei crater. Similarly, subaqueous landslides on Earth are initiated along a plane or curve that forms a headwall escarpment at the upslope margin. In many cases, the resulting deposit can be visually "fit" back into the erosional alcove, allowing for a crude reconstruction of the initial topography (Figure 9A). Other than the spatial correlation between the blocks and the crater rim, clear upslope alcoves in Galilaei crater are only present with the more recent landslides observed on the crater rim and in Tana Vallis (Figure 5). However, the absence of both surface tracks and well-oriented headwall escarpments can be explained by the age

of the crater. Persistent water has not been present on Mars for several billion years, and the intervening aeolian erosion could easily have resurfaced the crater wall morphology. Additionally, on both Earth and Mars, any track from the movement of a subaqueous landslide could have been covered over by pelagic sedimentation. The smooth crater floor surface, polygonal fractures in the crater base, and depressions surrounding some chaos blocks could be explained by lacustrine sedimentation after the emplacement of the blocks.

5.3. History of Formation

Based on the observed geomorphology, we propose a sequence of events for the formation of the Galilaei crater chaos terrain that was driven by subaqueous slope failure (Figure 10). After the initial impact, surface- and groundwater contributed to the infilling of Galilaei crater, forming a paleolake (per [23]).

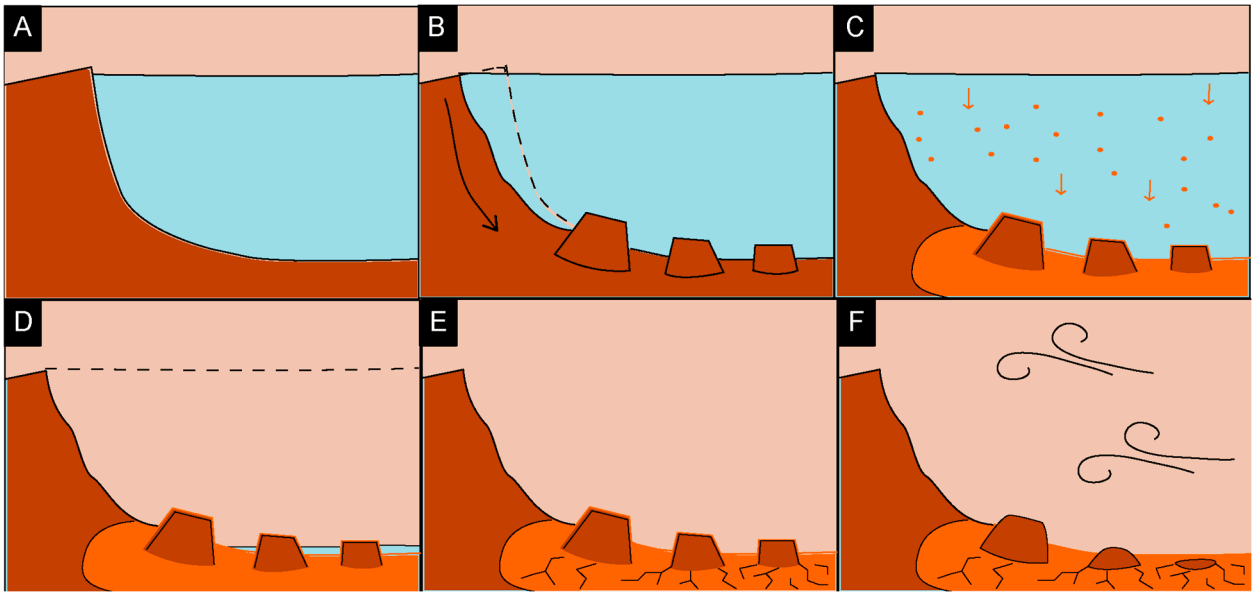

Figure 10. Schematic interpretation of the depositional history in Galilaei crater. (**A**) Galilaei crater hosts a paleolake with water levels near the crater rim before the development of any outflow channel. (**B**) Gravity-driven slope failures along the crater walls deposit slide blocks in the crater interior. (**C**) Pelagic sedimentation deposits flat-lying strata across the crater floor. (**D**) An outflow channel (Tana Vallis) is carved into the rim of Galilaei crater, causing it to rapidly drain. Some water remains in the lowest elevation regions in the center of the crater. (**E**) The remaining water evaporates from Galilaei crater, leaving polygonal desiccation patterns on the surface. (**F**) More than 1 billion years of intervening erosion degrade the surface expression of the blocks, causing some to round or be entirely winnowed away, leaving some pits in the lake deposits and leading to the morphologies observed today.

During a high stand in lake level, slope failures on the steep crater walls were initiated by impacts or other ground disturbance. Multiple, repeated slides led to the distribution of blocks observed on the crater floor today. Some larger (>1 km scale) blocks slide without significant deformation, or they fracture but preserved their original block shape. In other slides, some blocks were overturned, causing layered strata to become sub-vertically exposed (Figure 6D). After and between slope failure events, while water was still present within Galilaei crater, pelagic sedimentation of fines from the water column deposited material across the basin floor. This ultimately formed the crater floor unit and draped and filled in between the chaos blocks. This sedimentation covered evidence of the initial slide tracks and is bounded by the depth of depressions in the crater floor unit as at least several meters thick (Figure 7).

The water level eventually overtopped the crater wall, leading to rapid draining of the crater and the carving of Tana Vallis outflow channel (Figure 1) [23]. We argue that, as previously proposed, the draining of Galilaei crater must have occurred geologically rapidly, given the limited reworking observed on the surface of the chaos terrain blocks (Figure 6). Had the paleolake drained slowly, the tops of the chaos blocks would have been near the water surface for extended periods of time, and wave activity would have reworked the blocks, causing shoreline morphologies and eroding the supper surfaces. Such indicators are not present, further reinforcing the hypothesized rapid drain. Water not drained through Tana Vallis would have pooled in the bottom of the crater and eventually evaporated. Evaporation of the remnant lake water and subsequent desiccation of the crater floor formed the polygonal terrain observed in the crater bottom today (Figure 7). Since then, more than one billion years of aeolian erosion and impact resurfacing have degraded the interior of Galilaei crater. Some of the chaos blocks have been completely eroded away, leaving depressions in the polygonally fractured crater floor and exposing the material below the layer of lacustrine pelagic sedimentation (Figure 7B). Modern aeolian bedforms fill topographic lows, and ubiquitous martian dust covers the crater and its interior.

6. Conclusions

The chaos terrain in Galilaei crater, expressed as disorganized blocks at the base of the southeastern crater rim, formed vias subaqueous slope failure during a high-stand of the Galilaei paleo lake. The morphologies and distribution of the chaos blocks are analogous to subaqueous mass flows on Earth. This interpretation of Martian chaos terrain suggests that subsurface aquifers, ice melt, volcanic processes, or other mechanisms previously invoked for the formation of chaos terrain may not always be necessary to develop this landform, and highlights that no one mechanism can explain all chaos terrain on Mars. Gravity-driven subaqueous collapse of the crater wall provides a straightforward explanation for the morphologies observed in Galilaei crater and may serve as a model for interpreting chaos terrain in other closed paleolake basins.

Author Contributions: Conceptualization, M.D.; mapping N.N. and C.D.; analysis N.N. and C.D.; writing—original draft preparation, C.D. and N.N.; writing—review and editing, M.D., A.Y. and S.M. All authors have read and agreed to the published version of the manuscript.

Funding: This research received no external funding.

Data Availability Statement: All data used in this work are publicly archived on the NASA PDS. Shapefiles that can be used to reproduce the map in Figure 3 are archived on the PI's GitHub page here: https://github.com/GALE-Lab/NizamDivola2022_GalilaeiCrater_Mapping.

Acknowledgments: The authors thank J. Sneed and A. Fraeman for their assistance in analyzing CRISM data over the study area and the HiRISE team for collecting additional images of this area. The authors also thank four anonymous reviewers for their feedback on this work. N. Nizam and C. Divola worked as a team and were equal contributors to this work.

Conflicts of Interest: The authors declare no conflict of interest.

References

1. Breed, C.S.; Grolier, M.J.; McCauley, J.F. Morphology and distribution of common "sand" dunes on Mars—Comparison with the earth. *J. Geophys. Res.* **1979**, *84*, 8183–8204. [CrossRef]
2. Newsom, H.E.; Brittelle, G.E.; Hibbitts, C.A.; Crossey, L.J.; Kudo, A.M. Impact crater lakes on Mars. *J. Geophys. Res. Planets* **1996**, *101*, 14951–14955. [CrossRef]
3. Chan, M.A.; Netoff, D.I. A terrestrial weathering and wind abrasion analog for mound and moat morphology of Gale crater, Mars. *Geophys. Res. Lett.* **2017**, *44*, 4000–4007. [CrossRef]
4. Sharp, R.P.; Soderblom, L.A.; Murray, B.C.; Cutts, J.A. The surface of Mars 2. Uncratered terrains. *J. Geophys. Res.* **1971**, *76*, 331–342. [CrossRef]
5. Sharp, R.P. Mars: Fretted and chaotic terrains. *J. Geophys. Res.* **1973**, *78*, 4073–4083. [CrossRef]
6. Glotch, T.D.; Christensen, P.R. Geologic and mineralogic mapping of Aram Chaos: Evidence for a water-rich history. *J. Geophys. Res. Planets* **2005**, *110*. [CrossRef]

7. Meresse, S.; Costard, F.; Mangold, N.; Masson, P.; Neukum, G. Formation and evolution of the chaotic terrains by subsidence and magmatism: Hydraotes Chaos, Mars. *Icarus* **2008**, *194*, 487–500. [CrossRef]
8. Nummedal, D.; Prior, D.B. Generation of Martian chaos and channels by debris flows. *Icarus* **1981**, *45*, 77–86. [CrossRef]
9. Rodriguez, J.A.P.; Sasaki, S.; Kuzmin, R.O.; Dohm, J.M.; Tanaka, K.L.; Miyamoto, H.; Kurita, K.; Komatsu, G.; Fairén, A.G.; Ferris, J.C. Outflow channel sources, reactivation, and chaos formation, Xanthe Terra, Mars. *Icarus* **2005**, *175*, 36–57. [CrossRef]
10. Carr, M.H. Formation of Martian flood features by release of water from confined aquifers. *J. Geophys. Res. Solid Earth* **1979**, *84*, 2995–3007. [CrossRef]
11. Pedersen, G.B.M.; Head III, J.W. Chaos formation by sublimation of volatile-rich substrate: Evidence from Galaxias Chaos, Mars. *Icarus* **2011**, *211*, 316–329. [CrossRef]
12. Warner, N.H.; Gupta, S.; Kim, J.-R.; Muller, J.-P.; Le Corre, L.; Morley, J.; Lin, S.-Y.; McGonigle, C. Constraints on the origin and evolution of Iani Chaos, Mars. *J. Geophys. Res. Planets* **2011**, *116*. [CrossRef]
13. Leask, H.J.; Wilson, L.; Mitchell, K.L. Formation of Aromatum Chaos, Mars: Morphological development as a result of volcano-ice interactions. *J. Geophys. Res. Planets* **2006**, *111*. [CrossRef]
14. Rodriguez, J.A.P.; Sasaki, S.; Miyamoto, H. Nature and hydrological relevance of the Shalbatana complex underground cavernous system. *Geophys. Res. Lett.* **2003**, *30*. [CrossRef]
15. Wang, C.; Manga, M.; Wong, A. Floods on Mars released from groundwater by impact. *Icarus* **2005**, *175*, 551–555. [CrossRef]
16. Luzzi, E.; Rossi, A.P.; Massironi, M.; Pozzobon, R.; Maestrelli, D.; Corti, G. Chaotic Caldera collapse: A new interpretation for the origin of Chaotic terrains on Mars. In *EGU General Assembly Conference Abstracts*; European Geophysical Union: Vienna Austria, 2020; p. 11071.
17. Zegers, T.E.; Oosthoek, J.H.P.; Rossi, A.P.; Blom, J.K.; Schumacher, S. Melt and collapse of buried water ice: An alternative hypothesis for the formation of chaotic terrains on Mars. *Earth Planet. Sci. Lett.* **2010**, *297*, 496–504. [CrossRef]
18. Chapman, M.G.; Tanaka, K.L. Related Magma–Ice Interactions: Possible Origins of Chasmata, Chaos, and Surface Materials in Xanthe, Margaritifer, and Meridiani Terrae, Mars. *Icarus* **2002**, *155*, 324–339. [CrossRef]
19. Kargel, J.S.; Furfaro, R.; Prieto-Ballesteros, O.; Rodriguez, J.A.P.; Montgomery, D.R.; Gillespie, A.R.; Marion, G.M.; Wood, S.E. Martian hydrogeology sustained by thermally insulating gas and salt hydrates. *Geology* **2007**, *35*, 975–978. [CrossRef]
20. Melosh, H.J.; Ivanov, B.A. Impact Crater Collapse. *Annu. Rev. Earth Planet. Sci.* **1999**, *27*, 385–415. [CrossRef]
21. Barlow, N.G.; Boyce, J.M.; Costard, F.M.; Craddock, R.A.; Garvin, J.B.; Sakimoto, S.E.H.; Kuzmin, R.O.; Roddy, D.J.; Soderblom, L.A. Standardizing the nomenclature of Martian impact crater ejecta morphologies. *J. Geophys. Res. Planets* **2000**, *105*, 26733–26738. [CrossRef]
22. Tanaka, K.L.; Skinner, J.A., Jr.; Dohm, J.M.; Irwin, R.P., III; Kolb, E.J.; Fortezzo, C.M.; Platz, T.; Michael, G.G.; Hare, T.M. *Geologic Map of Mars: U.S. Geological Survey Scientific Investigations Map 3292, Scale 1:20,000,000, Pamphlet 43 p*; U.S. Geological Survey: Reston, VA, USA, 2014.
23. Coleman, N. Hydrographs of a Martian flood from the breach of Galilaei Crater. *Geomorphology* **2015**, *236*, 90–108. [CrossRef]
24. Malin, M.C.; Bell, J.F.; Cantor, B.A.; Caplinger, M.A.; Calvin, W.M.; Clancy, R.T.; Edgett, K.S.; Edwards, L.; Haberle, R.M.; James, P.B.; et al. Context Camera Investigation on board the Mars Reconnaissance Orbiter. *J. Geophys. Res. Planets* **2007**, *112*. [CrossRef]
25. Dickson, J.L.; Kerber, L.A.; Fassett, C.I.; Ehlmann, B.L. A Global, Blended CTX Mosaic of Mars with Vectorized Seam Mapping: A New Mosaicking Pipeline Using Principles of Non-Destructive Image Editing. In *Lunar and Planetary Science Conference*; Lunar and Planetary Institute: The Woodlands, TX, USA, 2018; Volume 49, pp. 1–2.
26. McEwen, A.S.; Eliason, E.M.; Bergstrom, J.W.; Bridges, N.T.; Hansen, C.J.; Delamere, W.A.; Grant, J.A.; Gulick, V.C.; Herkenhoff, K.E.; Keszthelyi, L.; et al. Mars Reconnaissance Orbiter's High Resolution Imaging Science Experiment (HiRISE). *J. Geophys. Res. Planets* **2007**, *112*. [CrossRef]
27. Smith, D.E.; Zuber, M.T.; Frey, H.V.; Garvin, J.B.; Head, J.W.; Muhleman, D.O.; Pettengill, G.H.; Phillips, R.J.; Solomon, S.C.; Zwally, H.J. Mars Orbiter Laser Altimeter: Experiment summary after the first year of global mapping of Mars. *J. Geophys. Res. Planets* **2001**, *106*, 23689–23722. [CrossRef]
28. Neukum, G.; Jaumann, R. HRSC: The high resolution stereo camera of Mars Express. In *Mars Express: The Scientific Payload*; Andrew Wilson, A., Ed.; ESA Publications Division: Noordwijk, The Netherlands, 2004; Volume 1240, pp. 17–35.
29. Murchie, S.; Arvidson, R.; Bedini, P.; Beisser, K.; Bibring, J.; Bishop, J.; Boldt, J.; Cavender, P.; Choo, T.; Clancy, R.T. Compact reconnaissance imaging spectrometer for Mars (CRISM) on Mars reconnaissance orbiter (MRO). *J. Geophys. Res. Planets* **2007**, *112*. [CrossRef]
30. Michael, G.G.; Neukum, G. Planetary surface dating from crater size–frequency distribution measurements: Partial resurfacing events and statistical age uncertainty. *Earth Planet. Sci. Lett.* **2010**, *294*, 223–229. [CrossRef]
31. Michael, G.G.; Platz, T.; Kneissl, T.; Schmedemann, N. Planetary surface dating from crater size–frequency distribution measurements: Spatial randomness and clustering. *Icarus* **2012**, *218*, 169–177. [CrossRef]
32. Michael, G.G. Planetary surface dating from crater size–frequency distribution measurements: Multiple resurfacing episodes and differential isochron fitting. *Icarus* **2013**, *226*, 885–890. [CrossRef]
33. Neukum, G.; Ivanov, B.A. Crater production function for Mars. In *Lunar and Planetary Science Conference*; Lunarand Planetary Institute: Woodlands, TX, USA, 2001; Volume 32.
34. Hartmann, W.K.; Neukum, G. Cratering chronology and the evolution of Mars. *Space Sci. Rev.* **2001**, *96*, 165–194. [CrossRef]

35. Ivanov, B.A. *Mars/Moon Cratering Rate Ratio Estimates BT—Chronology and Evolution of Mars*; Kallenbach, R., Geiss, J., Hartmann, W.K., Eds.; Springer: Dordrecht, The Netherlands, 2001; pp. 87–104.
36. Hartmann, W.K. Does crater "saturation equilibrium" occur in the solar system? *Icarus* **1984**, *60*, 56–74. [CrossRef]
37. Platz, T.; Michael, G.; Tanaka, K.L.; Skinner, J.A.; Fortezzo, C.M. Crater-based dating of geological units on Mars: Methods and application for the new global geological map. *Icarus* **2013**, *225*, 806–827. [CrossRef]
38. Hartmann, W.K.; Daubar, I.J. Martian cratering 11. Utilizing decameter scale crater populations to study Martian history. *Meteorit. Planet. Sci.* **2017**, *52*, 493–510. [CrossRef]
39. Mustard, J.F.; Murchie, S.L.; Pelkey, S.M.; Ehlmann, B.L.; Milliken, R.E.; Grant, J.A.; Bibring, J.P.; Poulet, F.; Bishop, J.; Dobrea, E.N.; et al. Hydrated silicate minerals on mars observed by the Mars reconnaissance orbiter CRISM instrument. *Nature* **2008**, *454*, 305–309. [CrossRef] [PubMed]
40. Fraeman, A.A.; Johnson, J.R.; Arvidson, R.E.; Rice, M.S.; Wellington, D.F.; Morris, R.V.; Fox, V.K.; Horgan, B.H.N.; Jacob, S.R.; Salvatore, M.R. Synergistic ground and orbital observations of iron oxides on Mt. Sharp and Vera Rubin ridge. *J. Geophys. Res. Planets* **2020**, *125*, e2019JE006294. [CrossRef] [PubMed]
41. Ceamanos, X.; Douté, S.; Fernando, J.; Schmidt, F.; Pinet, P.; Lyapustin, A. Surface reflectance of Mars observed by CRISM/MRO: 1. Multi-angle Approach for Retrieval of Surface Reflectance from CRISM observations (MARS-ReCO). *J. Geophys. Res. Planets* **2013**, *118*, 514–533. [CrossRef]
42. Balme, M.; Berman, D.C.; Bourke, M.C.; Zimbelman, J.R. Transverse Aeolian Ridges (TARs) on Mars. *Geomorphology* **2008**, *101*, 703–720. [CrossRef]
43. Berman, D.C.; Balme, M.R.; Rafkin, S.C.R.; Zimbelman, J.R. Transverse aeolian ridges (TARs) on Mars II: Distributions, orientations, and ages. *Icarus* **2011**, *213*, 116–130. [CrossRef]
44. Hartmann, W.K. Martian cratering III: Theory of crater obliteration. *Icarus* **1971**, *15*, 410–428. [CrossRef]
45. Chapman, C.R.; Jones, K.L. Cratering and obliteration history of Mars. *Annu. Rev. Earth Planet. Sci.* **1977**, *5*, 515–538. [CrossRef]
46. Smith, A.R.; Gillespie, D.R.; Montgomery, M.R. Efect of obliteration on crater-count chronologies for Martian surfaces. *Geophys. Res. Lett.* **2008**, *35*. [CrossRef]
47. Daubar, I.J.; McEwen, A.S.; Byrne, S.; Kennedy, M.R.; Ivanov, B. The current martian cratering rate. *Icarus* **2013**, *225*, 506–516. [CrossRef]
48. Hampton, M.A.; Lee, H.J.; Locat, J. Submarine landslides. *Rev. Geophys.* **1996**, *34*, 33–59. [CrossRef]
49. Locat, J.; Lee, H.J. Submarine landslides: Advances and challenges. *Can. Geotech. J.* **2002**, *39*, 193–212. [CrossRef]
50. Locat, J.; Lee, H.J.; Locat, P.; Imran, J. Numerical analysis of the mobility of the Palos Verdes debris avalanche, California, and its implication for the generation of tsunamis. *Mar. Geol.* **2004**, *203*, 269–280. [CrossRef]
51. Lee, H.J.; Kayen, R.E.; Gardner, J.V.; Locat, J. Characteristics of several tsunamigenic submarine landslides. In *Submarine Mass Movements and Their Consequences*; Springer: Dordrecht, The Netherlands, 2003; pp. 357–366.
52. Clague, D.A.; Moore, J.G. The proximal part of the giant submarine Wailau landslide, Molokai, Hawaii. *J. Volcanol. Geotherm. Res.* **2002**, *113*, 259–287. [CrossRef]
53. Moore, J.G.; Clague, D.A. Mapping the Nuuanu and Wailau landslides in Hawaii. *Washingt. DC Am. Geophys. Union Geophys. Monogr. Ser.* **2002**, *128*, 223–244.
54. Satake, K.; Smith, J.R.; Shinozaki, K. Three-Dimensional Reconstruction and Tsunami Model of the Nuuanu and Wailau Giant Landslides, Hawaii. *Hawaii Volcanoes Deep Underw. Perspect.* **2002**, *128*, 333–346.
55. Moore, J.G.; Normark, W.R.; Holcomb, R.T. Giant hawaiian landslides. *Annu. Rev. Earth Planet. Sci.* **1994**, *22*, 119–144. [CrossRef]
56. Normark, W.R.; Moore, J.G.; Torresan, M.E. Giant volcano-related landslides and the development of the Hawaiian Islands. In *Submarine Landslides: Selected Studies in the US Exclusive Economic Zone*; Geological Survey Bulletin US: Denver, CO, USA, 1993; Volume 2002, pp. 184–196.
57. Wessel, P.; Luis, J.F.; Uieda, L.; Scharroo, R.; Wobbe, F.; Smith, W.H.F.; Tian, D. The generic mapping tools version 6. *Geochem. Geophys. Geosyst.* **2019**, *20*, 5556–5564. [CrossRef]
58. Carlson, P.R. Holocene slump on continental shelf off Malaspina Glacier, Gulf of Alaska. *Am. Assoc. Pet. Geol. Bull.* **1978**, *62*, 2412–2426.
59. Coleman, J.M.; Prior, D.B.; Garrison, L.E. Submarine landslides in the Mississippi River delta. In *Offshore Technology Conference*; OnePetro: Houston, TX, USA, 1978.
60. McAdoo, B.G.; Pratson, L.F.; Orange, D.L. Submarine landslide geomorphology, US continental slope. *Mar. Geol.* **2000**, *169*, 103–136. [CrossRef]
61. Craddock, R.A.; Maxwell, T.A.; Howard, A.D. Crater morphometry and modification in the Sinus Sabaeus and Margaritifer Sinus regions of Mars. *J. Geophys. Res. Planets* **1997**, *102*, 13321–13340. [CrossRef]
62. Forsberg-Taylor, N.K.; Howard, A.D.; Craddock, R.A. Crater degradation in the Martian highlands: Morphometric analysis of the Sinus Sabaeus region and simulation modeling suggest fluvial processes. *J. Geophys. Res. Planets* **2004**, *109*. [CrossRef]
63. Lipman, P.W.; Normark, W.R.; Moore, J.G.; Wilson, J.B.; Gutmacher, C.E. The giant submarine alika debris slide, Mauna Loa, Hawaii. *J. Geophys. Res. Solid Earth* **1988**, *93*, 4279–4299. [CrossRef]
64. Masson, D.G.; Harbitz, C.B.; Wynn, R.B.; Pedersen, G.; Løvholt, F. Submarine landslides: Processes, triggers and hazard prediction. *Philos. Trans. R. Soc. A Math. Phys. Eng. Sci.* **2006**, *364*, 2009–2039. [CrossRef] [PubMed]